Effects of crosslinks on motor-mediated filament organization

Falko Ziebert¹, Igor S. Aranson¹, and Lev S. Tsimring²

E-mail: aronson@msd.anl.gov

- 1 Materials Science Division, Argonne National Laboratory, 9700 S Cass Avenue, Argonne, Illinois 60439, USA
- ² Institute for Nonlinear Science, University of California, San Diego, La Jolla, California 92093-0402, USA

Abstract. Crosslinks and molecular motors play an important role in the organization of cytoskeletal filament networks. Here we incorporate the effect of crosslinks into our model of polar motor-filament organization [Phys. Rev. E 71, 050901 (2005)], through suppressing the relative sliding of filaments in the course of motor-mediated alignment. We show that this modification leads to a nontrivial macroscopic behavior, namely the oriented state exhibits a transverse instability in contrast to the isotropic instability that occurs without crosslinks. This transverse instability leads to the formation of dense extended bundles of oriented filaments, similar to recently observed structures in actomyosin. This model also can be applied to situations with two oppositely directed motor species or motors with different processing speeds.

PACS numbers: 87.16.-b, 87.18.Hf, 05.65.+b

1. Introduction

Biological cells consist to a large degree of a complex, self-organizing viscoelastic fluid, the cytosol. Its main constituents include cytoskeletal proteins such as actin and tubulin, which exist mainly in the polymerized form as semi-flexible actin filaments and stiff microtubules [1, 2]. The entangled networks of microtubules and actin filaments form the cytoskeleton of most eukaryotic cells, stabilize their morphology and determine the rheological properties of the cytosol. These intricate networks are created and maintained by an efficient mechanism which involves various types of motor proteins as well as passive crosslinking proteins. Motors are specialized protein molecules that move along the cytoskeletal polymer scaffold and perform directed intracellular transport [3]. Additionally, if motors bind to more than one filament, they are able to move the filaments and reorganize the cytoskeleton itself. The crosslinks connect different filaments but do not move along them. Their main function is thus believed to provide rigidity and elasticity to the cytoskeleton.

Various experiments have been performed in recent years that shed light on the viscoelastic behavior of entangled cytoskeletal filament solutions, ranging from filament-motor mixtures [4], crosslinked filaments [5, 6, 7], and systems of filaments, motors and crosslinks [8]. Surprising new effects have been found such as active fluidization of actin gels by myosin motors [9].

Maintained in a state far from equilibrium, the active filaments exhibit a strong tendency towards self-organization. Bundles and contracting states have been found *in vitro* in actomyosin extracted from muscle cells [10], and various patterns like ray-like asters, spindle-like structures and rotating vortices have been reported in quasi two-dimensional mixtures of microtubules and motors [11, 12]. These dissipative structures have inspired many theoretical efforts [13, 14, 15, 16, 17, 18, 19] directed towards modeling active filament solutions.

While crosslinks so far have been mainly investigated only in the context of rheology, recently their influence on the dynamics and self-organization also attracted attention [20]. In particular, it was shown that crosslinks facilitate the formation of bundles in the actin-myosin system: at high concentration of adenosine triphosphate (ATP), actin-myosin systems display an isotropic phase; in the course of depletion of ATP however, myosin motors become static crosslinks and initiate the formation of oriented bundles and cluster-like patterns. Reintroduction of ATP in the bundled state resulted in consequent dissolution of the structures and reestablishment of the isotropic state.

Motivated by these experimental results, we focus here on the effects of static crosslinks on the self-organization of polar filaments and generalize the model for microtubule-motor interaction introduced in Refs. [17, 19]. In that model, the complicated process of filament interaction via multi-headed molecular motors was approximated by instant binary "inelastic collisions", leading to alignment of the filament orientation vectors and attraction between their centers of mass. Crosslinks alter these interaction rules. In particular, if two parallel filaments are cross-linked,

they are not able to slide past each other and become collocated. We model this effect here by suppressing relative sliding of the filaments in the course of alignment. Our analysis shows that this relatively minor modification produces a nontrivial macroscopic effect, namely the isotropic density instability of the polar oriented state of the filaments becomes transverse. In the nonlinear regime, this new kind of instability leads to the formation of dense oriented bundles, similar to those seen in experiments [20]. In contrast, the model without crosslinks demonstrates an isotropic instability in which density and orientation of the filaments are uncorrelated, and no bundling occurs.

2. Model

Here we outline the model of self-organization of microtubule-motor mixtures developed in our earlier works, Refs. [17, 19]. The microtubules are modeled as identical rigid polar rods of length L, and the molecular motors are introduced implicitly through corresponding interaction probabilities. Binary interactions of microtubules via multiheaded molecular motors are approximated by instant inelastic collisions leading to alignment of the microtubule orientation angles $\phi_{1,2}$ (or, equivalently, the unit vectors $\mathbf{n}_{1,2} = (\cos \phi_{1,2}, \sin \phi_{1,2})$) according to the following rules:

$$\begin{pmatrix} \phi_1^a \\ \phi_2^a \end{pmatrix} = \begin{pmatrix} \gamma & 1 - \gamma \\ 1 - \gamma & \gamma \end{pmatrix} \begin{pmatrix} \phi_1 \\ \phi_2 \end{pmatrix}. \tag{1}$$

Here $\phi_{1,2}^a$ are the orientations of the two rods after the collision, and the constant "restitution" parameter γ characterizes the inelasticity of the collision (in analogy to the restitution coefficient in granular media). The angle between the two rods is reduced after the collision by the "inelasticity" factor $\varepsilon = 2\gamma - 1$. Of special interest is the totally inelastic collision corresponding to $\gamma = 1/2$ or $\varepsilon = 0$. In this case the rods acquire the same orientation along the bisector $\bar{n} = (\cos \bar{\phi}, \sin \bar{\phi})$, and their center of mass positions, $r_{1,2}$, also align:

$$\phi_1^a = \phi_2^a = \bar{\phi} = \frac{\phi_1 + \phi_2}{2} \,, \tag{2}$$

$$r_1^a = r_2^a = \bar{r} = \frac{r_1 + r_2}{2}$$
 (3)

Here $\phi_{1,2}^a$ and $r_{1,2}^a$ are the orientation angles and the center of mass positions after the collision. We assume that the alignment through inelastic interaction occurs only if the initial angle difference $|\phi_1 - \phi_2|$ is smaller than a certain maximum interaction angle ϕ_0 . For $|\phi_1 - \phi_2| > \phi_0$, the angles and the positions are unchanged. The analysis of Refs. [17, 19] showed that in the spatially homogeneous case, the rods exhibited a spontaneous orientation transition if the density of the motors (or of the filaments) exceeded a critical density. Furthermore, for even higher densities, another instability was predicted which is isotropic and leads to inhomogeneous density variations.

The dynamics of this model can be described by the master equation for the probability distribution function $P(\mathbf{r}, \phi, t)$ to find a rod at position \mathbf{r} with orientation

 $\boldsymbol{n} = (\cos \phi, \sin \phi)$:

$$\frac{\partial P(\boldsymbol{r},\phi,t)}{\partial t} = \frac{\partial^2 P(\boldsymbol{r},\phi,t)}{\partial \phi^2} + \partial_i D_{ij} \partial_j P(\boldsymbol{r},\phi,t) + \mathcal{I}(\boldsymbol{r},\phi,t).$$
(4)

The first two terms on the right hand side describe rotational and translational diffusion, with an anisotropic diffusion matrix of the form

$$D_{ij} = \frac{1}{D_r} [D_{\parallel} n_i n_j + D_{\perp} (\delta_{ij} - n_i n_j)].$$
 (5)

The rotational, D_r , parallel, D_{\parallel} , and perpendicular, D_{\perp} , diffusion coefficients for rigid rods in a viscous fluid are well known [21]. The third term in Eq. (4) is the collision integral,

$$\mathcal{I}(\boldsymbol{r},\phi,t) = \int \int d\boldsymbol{r}_1 d\boldsymbol{r}_2 \int_{-\phi_0}^{\phi_0} d\phi_1 d\phi_2 W(\boldsymbol{r}_1 - \boldsymbol{r}_2, \boldsymbol{n}_1, \boldsymbol{n}_2) P(\boldsymbol{r}_1, \phi_1) P(\boldsymbol{r}_2, \phi_2)$$

$$\times \left[\delta(\phi - \phi_1^a) \delta(\boldsymbol{r} - \boldsymbol{r}_1^a) - \delta(\phi - \phi_1) \delta(\boldsymbol{r} - \boldsymbol{r}_1) \right],$$
(6)

where the localization of spatial interactions is introduced through a certain probabilistic kernel $W(\mathbf{r}_1 - \mathbf{r}_2, \mathbf{n}_1, \mathbf{n}_2)$ [17, 19].

The kernel W, expressing the probability of interaction between the rods as a function of the distance between their midpoints and their orientations, can be obtained from the following conditions: (i) since the size of motors is small compared to the length of filaments, two rods interact only if they intersect; (ii) due to translational and rotational invariance, the kernel depends only on differences $\phi_1 - \phi_2$ and $\mathbf{r}_1 - \mathbf{r}_2$; (iii) the kernel is invariant with respect to permutations $\mathbf{n}_1 \to \mathbf{n}_2$, $\mathbf{r}_1 \to \mathbf{r}_2$. The kernel can be represented as a product of two parts: a part W_0 which accounts for spatial localization due to the overlap condition of the filaments, and a part describing the motor-induced collision anisotropy.

The first part can be derived from the intersection condition between two rods with orientations $n_{1,2}$. It is easy to verify that the rods overlap if

$$|(\boldsymbol{r}_1 - \boldsymbol{r}_2) \times \boldsymbol{n}_1| \le L|\boldsymbol{n}_1 \times \boldsymbol{n}_2|/2, \tag{7}$$

$$|(\boldsymbol{r}_1 - \boldsymbol{r}_2) \times \boldsymbol{n}_2| \le L|\boldsymbol{n}_1 \times \boldsymbol{n}_2|/2 \tag{8}$$

holds. This overlap condition can be expressed in terms of discontinuous Θ -functions,

$$W_0 = W_n \Theta(L|\boldsymbol{n}_1 \times \boldsymbol{n}_2| - 2|(\boldsymbol{r}_1 - \boldsymbol{r}_2) \times \boldsymbol{n}_1|)\Theta(L|\boldsymbol{n}_1 \times \boldsymbol{n}_2| - 2|(\boldsymbol{r}_1 - \boldsymbol{r}_2) \times \boldsymbol{n}_2|), (9)$$

where W_n is a normalization constant, so that $\int W_0 d\mathbf{r} = 1$. Since this discontinuous kernel is difficult for calculations, the Θ -functions can be approximated by smooth Gaussians yielding

$$W_0(\mathbf{r}_1 - \mathbf{r}_2, \mathbf{n}_1, \mathbf{n}_2) \sim \exp \left[-4 \frac{((\mathbf{r}_1 - \mathbf{r}_2) \times \mathbf{n}_1)^2 + ((\mathbf{r}_1 - \mathbf{r}_2) \times \mathbf{n}_2)^2}{b^2 |\mathbf{n}_1 \times \mathbf{n}_2|^2} \right],$$
 (10)

where b is a cutoff length of order $b \lesssim L$. It is convenient to transform the kernel to the following representation (the integral of the kernel is normalized to 1):

$$W_0(\mathbf{r}_1 - \mathbf{r}_2, \psi) = \frac{4}{\pi b^2 \sin \psi} \exp \left[-\frac{2\mathbf{R}_{\parallel}^2}{b^2 \cos^2(\psi/2)} - \frac{2\mathbf{R}_{\perp}^2}{b^2 \sin^2(\psi/2)} \right] = W_0(\mathbf{R}, \psi), \quad (11)$$

where $\psi = \phi_1 - \phi_2$ is the difference of the orientation angles, and $\mathbf{R}_{\parallel} = (\mathbf{r}_1 - \mathbf{r}_2) \cdot \bar{\boldsymbol{n}}$ and $\mathbf{R}_{\perp} = -(\mathbf{r}_1 - \mathbf{r}_2) \times \bar{\boldsymbol{n}}$ are two vectors parallel and perpendicular to the bisector direction $\bar{\boldsymbol{n}}$. The cutoff length b introduced above can be estimated, for example, by comparison of the characteristic kernel width $\int \mathbf{R}^2 W_0(\mathbf{R}) d\mathbf{R}$ for the kernels given by Eqs. (9) and (10) for some typical angle, say $\psi = \pi/2$. Equating both integrals, one finds that $b^2/L^2 = 2/3$. ‡

Finally, the complete kernel can be represented in the form

$$W(\boldsymbol{r}_1 - \boldsymbol{r}_2, \boldsymbol{n}_1, \boldsymbol{n}_2) = gW_0(\boldsymbol{r}_1 - \boldsymbol{r}_2, \psi) \left(1 + \frac{\beta}{L} (\boldsymbol{r}_1 - \boldsymbol{r}_2) \cdot (\boldsymbol{n}_1 - \boldsymbol{n}_2) \right). \tag{12}$$

Here g is the interaction rate proportional to the motor density (which can be scaled away) and the last term $\propto \beta$ describes the anisotropic contribution to the kernel, which is associated to the increase of motor density towards the polar end of the filament due to dwelling of the motors. Accordingly, the constant β can be related to the dwell time [19].

Near the threshold of the orientation instability mentioned above, $\rho \gtrsim \rho_c$, the master equation can be systematically reduced to equations for the coarse-grained local density of filaments ρ and the coarse-grained local orientation τ

$$\rho = \int_{-\pi}^{\pi} P(\mathbf{r}, \phi, t) d\phi , \quad \boldsymbol{\tau} = \langle \boldsymbol{n} \rangle = \frac{1}{2\pi} \int \boldsymbol{n} P(\mathbf{r}, \phi, t) d\phi , \qquad (13)$$

by means of a bifurcation analysis.

3. Effects of crosslinks in the model

The effect of crosslinks on the motor-induced interaction of filaments is twofold. First, the simultaneous action of a static crosslink, serving as a hinge, and a motor moving along both filaments results in a fast and complete alignment of the filaments, as shown in Fig. 1. This justifies the assumption of fully inelastic collisions for the rods' interaction. Note that without crosslinks the overall change in the relative orientation of the filaments is much smaller: the angle between filaments decreases only by 25-30 % in average, see the discussion in Ref. [19]. Complete alignment also can occur for the case of simultaneous action of two motors moving in opposite direction, as in experiments on kinesin-NCD mixtures reported in Ref. [12], and even for two motors of the same type moving in the same direction but with a different speed due to variability of the properties and the stochastic character of the motion. Second, the crosslinks inhibit relative sliding of rods in the course of alignment, restricting the motion to rotation only. Thus, in contrast to the situation considered in Refs. [17, 19] and described by Eq. (3), in the presence of a crosslink the midpoints of the rods will not coincide after the interaction. In fact, the distances $S_{1,2}$ from the midpoints to the crosslink point do not change, as it is shown in Fig. 1.

‡ In our previous works [17, 19] we used a somewhat simpler expression for the kernel, $W_0 \sim \exp[-|\mathbf{r}_1 - \mathbf{r}_2|^2/b^2]$. As we have verified, this simplified approximation did not change the results on a qualitative level, affecting only numerical prefactors of some nonlinear terms.

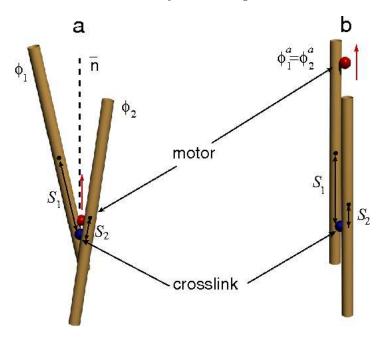


Figure 1. Sketch of the interaction between two filaments, a crosslink and a molecular motor. After the interaction, the motor (shown as a red sphere moving in the direction of the red arrow) aligns the filaments along the bisector \bar{n} , but the midpoint positions do not coincide due to the crosslink (blue sphere).

To describe the interaction rules in the presence of a crosslink, we express the radius-vector of an arbitrary point on a filament \mathbf{R}_i via the position of its midpoint \mathbf{r}_i , the filament orientation \mathbf{n}_i , and the distance from the center of mass S, $\mathbf{R}_i = \mathbf{n}_i S_i + \mathbf{r}_i$. The intersection point of two rods is given by the condition $\mathbf{R}^* = \mathbf{R}_1 = \mathbf{R}_2$, which fixes the values of $S_{1,2}$ to

$$S_{1,2} = \frac{(\mathbf{r}_2 - \mathbf{r}_1) \times \mathbf{n}_{2,1}}{\mathbf{n}_1 \times \mathbf{n}_2}.$$
 (14)

Due to the crosslink, the values of $S_{1,2}$ do not change during the interaction. Since the filaments become oriented along the bisector direction \bar{n} , the distance of the two filament midpoints from the total center of mass will be $\Delta S = (S_1 - S_2)$. Therefore, instead of Eqs. (2),(3) we obtain the interaction rules

$$\phi_1^a = \phi_2^a = \bar{\phi} = \frac{\phi_1 + \phi_2}{2} \,, \tag{15}$$

$$\boldsymbol{r}_{1,2}^{a} = \frac{\boldsymbol{r}_{1} + \boldsymbol{r}_{2}}{2} \pm \eta \frac{\bar{\boldsymbol{n}}\Delta S}{2} = \frac{\boldsymbol{r}_{1} + \boldsymbol{r}_{2}}{2} \pm \eta \frac{\bar{\boldsymbol{n}}((\boldsymbol{r}_{1} - \boldsymbol{r}_{2}) \cdot \bar{\boldsymbol{n}})}{2\cos\psi}.$$
 (16)

Here we have introduced the parameter η interpolating between two cases: the case with crosslinks present corresponds to $\eta = 1$; for $\eta = 0$ the previous model, Eqs. (2),(3), is recovered. Thus the value of η can be roughly interpreted as the effective strength of crosslinks or an effective fraction of crosslinks with respect to motors.

The interaction rules, Eqs. (15) and (16), can be used to evaluate the collision integral, Eq.(6). Omitting lengthy calculations (see the Appendix for details) after expanding the master equation (4) near the threshold of the orientation instability, we

arrive at the following set of nonlinear equations for the coarse-grained density ρ and orientation τ :

$$\partial_{t}\rho = D_{\rho}\nabla^{2}\rho - \zeta\nabla^{4}\rho - \frac{\phi_{0}B^{2}}{64\pi}\left(1 - \eta^{2}\right)\nabla^{2}\rho^{2}$$

$$-\frac{\pi\phi_{0}B^{2}}{16}\left[\left(S[\phi_{0}] + (1 - 2S[\phi_{0}])\eta^{2}\right)\nabla^{2}\boldsymbol{\tau}^{2} + 2\left(S[\phi_{0}] - \eta^{2}\right)\partial_{i}\partial_{j}(\tau_{i}\tau_{j})\right], \qquad (17)$$

$$\partial_{t}\boldsymbol{\tau} = \epsilon(\rho - \rho_{c})\boldsymbol{\tau} - A|\boldsymbol{\tau}|^{2}\boldsymbol{\tau} + D_{\tau_{1}}\nabla^{2}\boldsymbol{\tau} + D_{\tau_{2}}\nabla\nabla\cdot\boldsymbol{\tau} + \frac{B^{2}\rho_{0}}{4\pi}\nabla^{2}\boldsymbol{\tau}$$

$$-H\left[\frac{1}{16\pi}\nabla\rho^{2} - \left(\pi - \frac{8}{3}\right)\boldsymbol{\tau}(\nabla\cdot\boldsymbol{\tau}) - \frac{8}{3}(\boldsymbol{\tau}\cdot\nabla)\boldsymbol{\tau}\right], \qquad (18)$$

with $S[x] = \sin(x)/x$ and B = b/L. The constants A, ϵ and the critical density ρ_c are functions of the maximum interaction angle ϕ_0 and the inelasticity coefficient γ :

$$A = 2\phi_0 \frac{\left(S[\phi_0(2\gamma - 1)] - S[\phi_0]\right) \left(S[\phi_0(\gamma + 1)] + S[\phi_0(\gamma - 2)] - S(2\phi_0) - S(\phi_0)\right)}{2/\phi_0 - \left(S[2\phi_0(\gamma - 1)] + S[2\phi_0\gamma] - S[2\phi_0] - 1\right)\rho/2\pi}$$

$$\epsilon = \frac{\phi_0}{\pi} \left[S[\phi_0(\gamma - 1)] + S[\phi_0\gamma] - S(\phi_0) - 1\right], \quad \rho_c = \frac{1}{\epsilon}. \tag{19}$$

In the following we consider the case $\phi_0 = \pi$ as motivated below. Then the density equation (17) becomes somewhat simpler since $S[\phi_0] = 0$. We have introduced rescaled diffusion coefficients, namely $D_{\rho} = (D_{\parallel} + D_{\perp})/(2D_rL^2) = 1/32$, $D_{\tau_1} = (D_{\parallel} + 3D_{\perp})/(4D_rL^2) = 5/192$ and $D_{\tau_2} = (D_{\parallel} - D_{\perp})/(2D_rL^2) = 1/96$. In order to scale out the motor density g we rescaled density and orientation vector, $g\rho \to \rho$, $g\tau \to \tau$. Also length is normalized by $\mathbf{r} \to \mathbf{r}/L$ and time by $t \to t/D_rL^2$. The anisotropic contribution proportional to $H = \beta b^2/L^2 = \beta B^2$ is due to the polar distribution of the motors along the interacting filaments, while the anisotropic contribution in the ρ -equation is due to the crosslinks. The isotropic higher order diffusion term $\zeta \nabla^4 \rho$ was included for regularization purposes of the equation at very short wavelengths. Assuming additionally $\gamma = 1/2$ (i.e. totally inelastic collisions, as justified above), one obtains from Eqs. (19): $\epsilon = 4/\pi - 1 \approx 0.273$, $A \approx 2.18$ and the critical density $\rho_c \approx 3.663$.

A sketch of the phase diagram for Eqs. (17), (18) in the plane of the motor-induced anisotropy parameter H and the mean density ρ_0 is shown in Fig. 2. A uniform isotropic state, $\rho = \rho_0$ and $\tau = 0$, loses its stability if $\rho_0 > \rho_c$, independent of the value of H. In the spatially uniform case, orientation modulations grow into a polar state with nonzero $|\tau| = [\epsilon(\rho_0 - \rho_c)/A]^{1/2}$ and arbitrary orientation of τ . Recall that the density ρ_0 is scaled by the "collision rate" g, and thus is proportional to both the density of tubules and the density of motors. This implies that either increasing the number of motors or the number of filaments can induce the polar phase. However, in extended systems, the growth of spatially inhomogeneous modes leads to the formation of a complex state characterized by disordered arrays of vortices or asters depending on the value of the anisotropy parameter H; the stability limit of vortices, indicated by the black solid line, terminates at a critical point at $H = H_c$. The vortex-aster-competition is governed

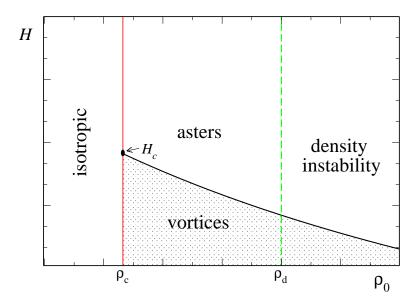


Figure 2. Sketch of the phase diagram of the rescaled density ρ_0 (being the product of motor and filament density) against anisotropy parameter H in the absence of crosslinks. Above ρ_c , the polar state is formed. Beyond ρ_d , given by Eq. (22), an isotropic density instability occurs. Depending on parameters, the density instability may happen also prior to the orientation instability, i.e. $\rho_d < \rho_c$. In between ρ_c and ρ_d , asters are stable above the critical line (solid black line) while vortices are linearly stable below this line. The critical line terminates at the point $H = H_c$. In the presence of crosslinks, for $\phi_0 = \pi$ bundles occur throughout the polar phases, i.e. beyond the red line. However, they are in nonlinear coexistence with the asters/vortices.

predominantly by the τ -equation, Eq. (18), and thus prevails whether crosslinks are present or not. In the case without crosslinks, $\eta = 0$, for densities $\rho > \rho_d$, the homogeneous oriented state loses its stability with respect to density fluctuations as implied by the green dashed line in Fig. 2. If crosslinks are present however, $\eta = 1$, the density instability is (to leading order) independent of the value of filament density and thus bundles can be found throughout the polar phase, i.e. for all $\rho > \rho_c$, where they are in complicated nonlinear competition with the aster and vortex defects.

4. Instability of the homogeneous polar state

For $\eta = 0$, Eqs. (17),(18) reduce to the model without crosslinks studied in Refs. [17, 19]. As it was shown in [17, 19], this equation exhibits an isotropic density instability if $\rho > \rho_d$ as calculated below. In the presence of crosslinks ($\eta = 1$), the term in Eq. (17) proportional to $\nabla^2 \rho^2$ which is responsible for the density instability vanishes, and instead a new anisotropic term $\partial_i \partial_j (\tau_i \tau_j)$ appears. This term couples the density and orientation perturbations already in the linear order. As we will show in the following, this new

crosslink-induced anisotropic coupling modifies the density instability so it becomes transverse to the direction of polar orientation (in both the linear and nonlinear regime).

Let us investigate the linear stability of the homogeneous polar solution of Eqs. (17) and (18), describing a state with density ρ_0 and polar orientation $\boldsymbol{\tau}_0$ given by $\epsilon(\rho - \rho_c) = A|\boldsymbol{\tau}_0|^2$. Without loss of generality we set $\boldsymbol{\tau}_0$ along x-direction, $\boldsymbol{\tau}_0 = (|\boldsymbol{\tau}_0|, 0)$. Linearizing the model equations around this state by making the ansatz $\{\rho, \tau_x, \tau_y\} = \{\rho_0, \tau_0, 0\} + \{\delta\rho, \delta\tau_x, \delta\tau_y\} \exp[\sigma(\boldsymbol{k})t + ik_xx + ik_yy]$, one can deduce the linear growth rates σ as a function of the modulation wavenumbers k_x, k_y . For simplicity we set H = 0 here. Finite but small values of H introduce a small drift but only slightly affect the growth rates.

First consider the case without crosslinks ($\eta = 0$). Then Eqs. (17),(18) reduce to the model of Refs. [17, 19]. There are three linear modes in the system. The two largest growth rates for long-wave perturbations are associated to a transverse orientational mode and to a mixed density-orientation mode. The third mode, related to the modulus of the orientation, is always damped. To leading order in k_x , k_y the transverse orientational mode reads

$$\sigma_{\tau} = -\left(D_{\tau_1} + \frac{B^2 \rho_0}{4\pi}\right) k_x^2 - \left(D_{\tau_1} + D_{\tau_2} + \frac{B^2 \rho_0}{4\pi}\right) k_y^2, \tag{20}$$

and is thus always damped. For the mixed density mode one obtains

$$\sigma_{\rho} = -\left(D_{\rho} - \frac{B^2 \rho_0}{32}\right) (k_x^2 + k_y^2). \tag{21}$$

Thus a density instability occurs at

$$\rho_0 > \rho_d = \frac{32D_\rho}{B^2} \,, \tag{22}$$

as already described in Refs. [17, 19], which to leading order is isotropic. Note that depending on the model parameters the density instability for $\eta = 0$ may also occur prior to the orientation instability, i.e. ρ_d can be smaller than ρ_c .

A similar analysis can be done in the presence of crosslinks, $\eta = 1$. While the orientational mode remains unchanged, for the mixed density mode one now obtains

$$\sigma_{\rho} = -\left(D_{\rho} + \frac{B^2 \pi^2 \epsilon}{16A}\right) k_x^2 - \left(D_{\rho} - \frac{B^2 \pi^2 \epsilon}{16A}\right) k_y^2. \tag{23}$$

For perturbations in x-direction, i.e. parallel to the polar orientation, the density mode is damped. However, using the estimates from above, $\epsilon \approx 0.273$, A = 2.18, $D_{\rho} = 1/32$, and $B^2 \approx 2/3$, one obtains that the coefficient in front of k_y is negative: $D_{\rho} - \frac{B^2 \pi^2 \epsilon}{16A} < 0$, i.e. transverse perturbations (i.e. with small k_x and finite k_y) are unstable.

Although this linear analysis reveals the possibility of a transverse instability in the presence of crosslinks, it is not clear if the density modulations perpendicular to the filament orientation really lead to bundle-like structures in the nonlinear regime. To investigate the long-term development of this instability, we performed numerical simulations of the full set of equations (17),(18), as described below.

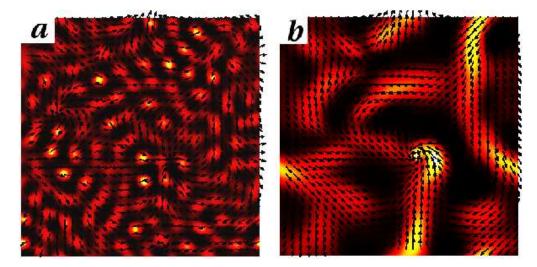


Figure 3. Composite image of the density (color code: black low density, bright yellow high density) and the filament orientation field (arrows). a) The model of Ref. [19] ($\eta = 0$) for $\rho_0 = 5$ in the region of the isotropic density instability. Here the filament orientation is uncorrelated with the density gradient. b) The model with crosslinks ($\eta = 1$) for a density of $\rho_0 = 6$ displays pronounced bundles, and the local filament orientation is predominantly along the bundles. Other parameters values: $H = 0.005, B^2 = 0.6, \zeta = 0.04$.

5. Numerical studies

In order to study the system beyond the linear regime, we performed numerical investigations of Eqs. (17),(18). The studies were conducted in a $80L \times 80L$ periodic domain, for different values of the parameter η characterizing the concentration of crosslinks. Small amplitude noise was used as an initial condition for the τ field, and $\rho = \rho_0 + \text{noise}$ for the density field. Representative results for $\eta = 0, 1$ are presented in Fig. 3. In both situations, the simulations were performed in the regime where the homogeneous oriented state is unstable with respect to density fluctuations. However, depending on the value of the parameter η , the manifestation of the instability is different. For $\eta = 0$ (without crosslinks), the numerical solution shows that the filament orientation and density gradients are mostly uncorrelated, cf. Fig. 3a.

In contrast, for $\eta=1$ (with crosslinks), we observed that the instability indeed resulted in the formation of anisotropic bundles with the filaments' orientation predominantly along the bundles, as shown in Fig. 3b. The bundles show a tendency to coarsen with time: small bundles coalesce into bigger bundles. The overall pattern is reminiscent of experimental observations of self-organization in both microtubules interacting with a mixture of motors of two different directions (kinesin and NCD) [12] and experiments on actomyosin where ATP-depleted myosin motors become crosslinks, cf. Fig. 4.

In order to characterize the degree of alignment quantitatively, we calculated the

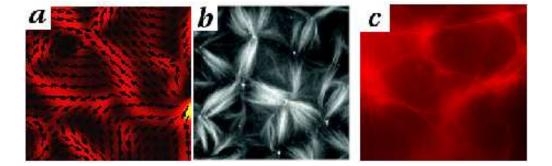


Figure 4. a) Composite image of the density (color code: black low density, red high density) and orientation field (arrows) for the model with crosslinks, same parameters as in Fig. 3b but at an early stage of evolution. b) Structure observed in microtubule-kinesin-NCD mixtures from *Surrey et al.* [12]. Here the two oppositely directed motors can be effectively mapped to the case of motor and crosslink. c) Experiment on actomyosin by *Smith et al.*, where ATP-depleted oligomeric myosin-motors become crosslinks [20].

alignment coefficient between the density gradient $\nabla \rho$ and the orientation τ :

$$C = 2\langle \sin^2(\phi_\rho - \phi_\tau) \rangle - 1, \qquad (24)$$

where ϕ_{ρ} and ϕ_{τ} are the angles between $\nabla \rho$ and the x-axis and $\boldsymbol{\tau}$ and the x-axis correspondingly. The alignment coefficient C=1 if the vectors $\nabla \rho$ and $\boldsymbol{\tau}$ are everywhere perpendicular, and C=-1 if they are parallel or antiparallel.

We find an alignment coefficient of C = -0.0045 for the image shown in Fig. 3a and corresponding to $\eta = 0$ (no crosslinks), confirming that the fields τ and $\nabla \rho$ are practically uncorrelated. For the situation shown in Fig. 3b and corresponding to $\eta = 1$ (crosslinks), we obtained a much larger value of $C \approx 0.188$, implying that the density gradient and the orientation are predominantly orthogonal. That means that density modulations are transverse to the orientation within a bundle.

6. Conclusions

As we have demonstrated above, the effect of crosslinks on the organization of polar filaments is twofold. First, the crosslinks, acting as hinges, allow zipping and result in the alignment of polar filaments by directional motion of molecular motors. Second, the ensuing polar state is unstable with respect to transverse density perturbations yielding bundles of oriented filaments, in contrast to the case without crosslinks in which the density instability is isotropic.

This result has a simple physical interpretation. In the absence of crosslinks the motors tend to bring together the mid-point positions of microtubules, triggering an isotropic density instability. This instability is a direct counterpart of the aggregation or clustering in a gas of inelastic or sticky particles [23]. With a crosslink holding two filaments together at the intersection point, however, the motion of the filaments along the bisector is suppressed whereas the angular aggregation proceeds unopposed

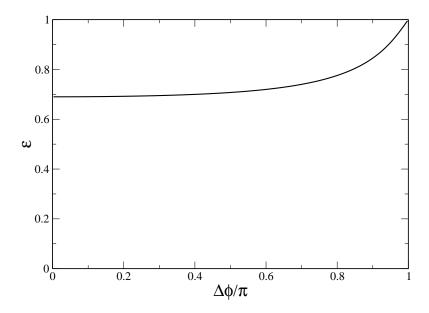


Figure 5. The effective inelasticity factor ε as a function of the initial angle between two rigid filaments $\Delta \phi / \pi$, see for detail Ref. [19].

(furthermore, in fact it becomes much more effective). Thus crosslinks turn the isotropic instability into a transversal one.

There are two experiments related to the model described here. The experiments on microtubules in the presence of two oppositely directed motor species, as reported in Ref. [12], appear to produce the same qualitative result as the case of a single motor species mixed with crosslinks. This is because two motors moving from an initial intersection point in opposite directions along filaments also lead to their complete alignment. Additionally, our analysis possibly sheds new light on the interpretation of recent experiments by Smith *et al.* [20] on actin - myosin mixtures. In this experiment, no patterns were observed in a situation with abundant ATP. However, long dense bundles of actin filaments were observed when ATP was depleted by the multi-headed myosin motor constructs, for which it is known that in the absence of ATP they rigidly attach to the actin filaments and effectively become static crosslinks. Also in accordance with this interpretation, reinjection of ATP into the motor-filament solution resulted in a consequent dissolution of the bundles and homogenized the system anew.

This experimental result can be interpreted as follows. As mentioned earlier, in the absence of crosslinks, the interaction of one motor with a filament pair does not result in complete alignment. In fact, the average decrease of the relative angle is of the order of 25-30% only, corresponding to a value of the restitution coefficient of $\gamma \approx 0.85$ or to a value of the effective inelasticity factor $\varepsilon = 2\gamma - 1 \approx 0.7$. Since the inelasticity factor approaches 1 at large ψ (see Fig. 5), it effectively produces a cutoff interaction

angle of the order of $\phi_0 \approx 0.6\pi$. Filament flexibility only slightly decreases this value [22]. Using the above values for γ and ϕ_0 , one finds from Eq. (19) that the critical density needed for the orientational instability is about $\rho_{c0} \approx 15.7$. However, in the presence of crosslinks, the interaction becomes fully inelastic, and is described by the restitution coefficient $\gamma = 1/2$. Also, the interaction leads to a complete alignment for any initial angle, so we can take $\phi_0 = \pi$. The critical density for these conditions $(\gamma = 1/2, \phi_0 = \pi)$ is $\rho_{c1} \approx 3.66$, which is more then four times smaller. Thus in the experiments, even if without crosslinks the motor density was not high enough to trigger the orientation transition, due to the crosslinking by ATP-depleted motors the system is likely driven beyond the threshold of orientation transition. Moreover, the oriented state is typically unstable with respect to a transverse instability leading to bundle formation, implying that bundles are competing with aster-like structures as the experimental pictures suggest.

The inclusion of crosslinks in the model of filament interaction via molecular motors, Ref. [17], was straightforward and yielded nontrivial results. However, further generalizations of the model are needed. First, instead of the parameter η interpolating between the cases with and without crosslinks, an additional field for the density of crosslinks should be introduced. In case of the actomyosin system, where ATP-depleted motors are acting like crosslinks, this field might be coupled via some simple reaction kinetics to the active motor density. Second, the role of filament flexibility is worth investigating in some detail (cf. [22]). Furthermore, it is well known that in vivo, the cytoskeletal filaments are often met in a state of constant polymerization and depolymerization by means of ATP and GTP hydrolysis, another nonequilibrium process that is known to lead to structure formation [24, 25, 26]. The competition of the two main nonequilibrium processes in the cytoskeleton, active transport of the filaments by molecular motors and active polymerization of the filaments themselves, might lead to new and surprising behavior. Finally, an analysis of the homogeneous polar state in a filament-motor model with motor-induced drift, which we have neglected here, is adressed in Ref. [27].

We thank David Smith and Joseph Käs for stimulating discussions and for providing panel c) of Fig. 4. This work was supported by the US DOE, grant DE-AC02-06CH11357.

7. Appendix: Evaluation of the collision integral

The first term of the collision integral, Eq. (6), can be simplified by integrating out the δ -function after having expressed ϕ_1 by $\phi_1 = 2\phi - \phi_2$ and \mathbf{r}_1 by

$$\boldsymbol{r}_1 = \boldsymbol{r} + \frac{\cos(\psi/2)}{\eta + \cos(\psi/2)} (\boldsymbol{r} - \boldsymbol{r}_2) - \frac{\eta}{\eta + \cos(\psi/2)} \hat{A} (\boldsymbol{r} - \boldsymbol{r}_2), \qquad (25)$$

where $\psi = \phi_1 - \phi_2$ as defined in the main text and where we have introduced the matrix

$$\hat{A} = \begin{pmatrix} \cos(2\bar{\phi}) & \sin(2\bar{\phi}) \\ \sin(2\bar{\phi}) & -\cos(2\bar{\phi}) \end{pmatrix}. \tag{26}$$

(Note that after integrating over $\delta(\phi - \bar{\phi})$ the angle in the matrix \hat{A} becomes ϕ .) Then one substitutes $w = 2(\phi - \phi_2)$ and $\boldsymbol{\xi} = \boldsymbol{r}_1 - \boldsymbol{r}_2$.

In the second term the δ -function leads to $\phi = \phi_1$. After the suitable substitution $w = \phi - \phi_2$ this implies $\bar{\phi} = \phi - w/2$. Finally one obtains the following simple form

$$\mathcal{I} = \int d\boldsymbol{\xi} \int_{-\phi_0}^{\phi_0} dw W(\boldsymbol{\xi}, w) \left[P(\boldsymbol{r} + \hat{A}_1 \boldsymbol{\xi}, \phi + w/2) P(\boldsymbol{r} - \hat{A}_2 \boldsymbol{\xi}, \phi - w/2) - P(\boldsymbol{r}, \phi) P(\boldsymbol{r} - \boldsymbol{\xi}, \phi - w) \right], \tag{27}$$

with

$$\hat{A}_1 = \frac{2\cos(w/2)\hat{1} - \eta(\hat{1} + \hat{A})}{4\cos(w/2)} , \quad \hat{A}_2 = \frac{2\cos(w/2)\hat{1} + \eta(\hat{1} + \hat{A})}{4\cos(w/2)}.$$
 (28)

In case of $\eta = 0$, i.e. in the absence of crosslinks, one regains $\hat{A}_1 = \hat{A}_2 = 1/2$ as in the model of Ref. [19].

To evaluate the spatial integral, one has to transform to the coordinates $\mathbf{R} = (R_{\parallel}, R_{\perp})$ introduced in the kernel, Eq. (11). These are connected to $\boldsymbol{\xi}$ via a simple rotation,

$$\begin{pmatrix} \mathbf{R}_{\parallel} \\ \mathbf{R}_{\perp} \end{pmatrix} = \hat{R}_{\bar{\phi}} \begin{pmatrix} \xi_x \\ \xi_y \end{pmatrix}, \quad \hat{R}_{\bar{\phi}} = \begin{pmatrix} \cos \bar{\phi} & \sin \bar{\phi} \\ -\sin \bar{\phi} & \cos \bar{\phi} \end{pmatrix}, \tag{29}$$

and the collision integral becomes

$$\mathcal{I} = \int dR_{\parallel} dR_{\perp} \int_{-\phi_0}^{\phi_0} dw W(\mathbf{R}, w) \Big[P(\mathbf{r} + \hat{A}_1 \hat{R}_{\phi} \boldsymbol{\xi}, \phi + w/2) P(\mathbf{r} - \hat{A}_2 \hat{R}_{\phi} \boldsymbol{\xi}, \phi - w/2) - P(\mathbf{r}, \phi) P(\mathbf{r} - \hat{R}_{\phi - w/2} \boldsymbol{\xi}, \phi - w) \Big].$$
(30)

8. References

- H. Lodish, A. Berk, S. L. Zipursky, P. Matsudaira, D. Baltimore and J. Darnell, Molecular Cell Biology, W. H. Freeman, New York (1999).
- [2] B. Alberts, A. Johnson, J. Lewis, M. Raff, K. Roberts and P. Walter, *Molecular Biology of the Cell*, Garland Publishing, New York (2001).
- [3] J. Howard, Mechanics of Motor Proteins and the Cytoskeleton, Sinauer, Sunderland (2001).
- [4] L. LeGoff, F. Amblard and E. Furst, Phys. Rev. Lett. 88, 018101 (2002).
- F. C. MacKintosh, J. Käs and P. A. Janmey, Phys. Rev. Lett. 75, 4425 (1995).
- [6] C. Storm, J. J. Pastore, F. C. MacKintosh, T. C. Lubensky, P. A. Janmey, Nature 435, 191 (2005).
- [7] M. Gardel, F. Nakamura, J. Hartwig, T. Stossel and D. Weitz, Proc. Natl. Acad. Sci. USA 103, 1762 (2006).
- [8] D. Mizuno, C. Tardin, C. F. Schmidt and F. C. MacKintosh, Science 315, 370 (2007).
- [9] D. Humphrey, C. Duggan, D. Saha, D. Smith and J. Käs, Nature 416, 413 (2002).
- [10] K. Takiguchi, J. Biochem. 109, 520 (1991).
- [11] F. J. Nédélec, T. Surrey, A. C. Maggs and S. Leibler, Nature 389, 305 (1997).
- [12] T. Surrey, F. Nédélec, S. Leibler and E. Karsenti, Science 292, 116 (2001).
- [13] H. Nakazawa and K. Sekimoto, J. Phys. Soc. Japan 65, 2404 (1996).
- [14] H. Y. Lee and M. Kardar, Phys. Rev. E 64, 056113 (2001).
- [15] T. B. Liverpool and M. C. Marchetti, Phys. Rev. Lett. 90, 138102 (2003).
- [16] K. Kruse, J. F. Joanny, F. Jülicher, J. Prost and K. Sekimoto, Phys. Rev. Lett. 92, 078101 (2004).

- [17] I. S. Aranson and L. S. Tsimring, Phys. Rev. E 71, 050901 (2005).
- [18] F. Ziebert and W. Zimmermann, Eur. Phys. J. E 18, 41 (2005).
- [19] I. S. Aranson and L. S. Tsimring, Phys. Rev. E 74, 031915 (2006).
- [20] D. Smith, F. Ziebert, D. Humphrey, C. Duggan, M. Steinbeck, W. Zimmermann and J. Käs, Molecular motor-induced instabilities and crosslinkers determine biopolymer organization, Biophys. J. (2007), in press.
- [21] M. Doi and S. F. Edwards, The Theory of Polymer Dynamics, Clarendon Press, Oxford (1986).
- [22] D. Karpeev, I. S. Aranson, L. S. Tsimring and H. Kaper, *Interaction of Semi-flexible Filaments and Molecular Motors*, submitted to Phys. Rev. E (2007).
- [23] I.S. Aranson and L.S. Tsimring, Rev. Mod. Phys. 78, 641 (2006).
- [24] E. Mandelkow, E.-M. Mandelkow, H. Hotani, B. Hess and S. C. Müller, Science, 246, 1291 (1989).
- [25] M. Hammele and W. Zimmermann, Phys. Rev. E 67, 021903 (2003).
- [26] F. Ziebert and W. Zimmermann, Phys. Rev. E **70**, 022902 (2004).
- [27] R. Peter, V. Rühle, F. Ziebert and W. Zimmermann, New J. Phys., same issue (2007).